Statistical Modeling and Experimental Verification of Wideband MIMO Mobile-to-mobile Channels in Highway Environments

Alenka G. Zajić *, Gordon L. Stüber *, Thomas G. Pratt †, and Son Nguyen §
* School of Electrical and Computer Engineering Georgia Institute of Technology, Atlanta, GA 30332 USA
†Georgia Tech Research Institute, Atlanta, GA 30332 USA
§ Army Research Laboratory, Adelphi, MA 20783 USA

***Abstract*— A three-dimensional reference model for wideband multiple-input multiple-output (MIMO) mobile-to-mobile (M-to-M) channels is reviewed. To validate the reference model, an experimental MIMO M-to-M channel-sounding campaign was conducted for M-to-M vehicular communication with vehicles travelling along expressways in a metropolitan area. The measured data is processed and the channel statistics obtained from the reference model and from the empirical measurements are compared. The close agreement between the analytically and empirically obtained channel statistics confirms the utility of the proposed reference model.**

I. Introduction

Mobile-to-mobile (M-to-M) communications play an important role in mobile ad-hoc wireless networks, intelligent transportation systems, and relay-based cellular networks. The statistical properties of M-to-M channels are quite different from conventional fixed-to-mobile cellular land mobile radio channels [1]. M-to-M communication systems are equipped with low elevation antennas and have both the transmitter (T_x) and receiver (R_x) in motion. Akki and Haber [1] proposed a two-dimensional (2-D) reference model for single-input single-output (SISO) M-to-M Rayleigh fading channels. Channel sounding measurements for narrow-band and wide-band SISO M-to-M channels have been reported in [2], [3], respectively. The reference model for narrow-band multiple-input multiple-output (MIMO) M-to-M channels has been proposed in [4], based on 2-D radio propagation. All previously reported models are two-dimensional and accurate only for certain environments, e.g., rural areas. For urban environments, the tree-dimensional (3-D) models are more appropriate. Hence, we have recently proposed the 3-D reference models for *narrowband* and *wideband* MIMO M-to-M multipath fading channels [5], [6]. We have also derived the first- and second-order statistics for the proposed models [6], [7] along with simulation models [8].

0
Prepared through collaborative participation in the Collaborative Technology Alliance for Communications & Networks sponsored by the U.S. Army Research Laboratory under Cooperative Agreement DAAD19-01-2-0011. The U.S. Government is authorized to reproduce and distribute reprints for Government purposes notwithstanding any copyright notation thereon.

This paper verifies our 3-D wideband MIMO M-to-M reference model in [6] by using MIMO M-to-M channel measurements collected from vehicles travelling along the Interstate highways near the midtown Atlanta metropolitan area. First, we review our reference model. Then, we describe the measurement campaign and the data processing techniques used to process the measured data. Finally, we compare the space-Doppler power spectral density (sD-psd) and the power space-delay spectral density (psds) obtained from the reference model with those obtained from the measured data. The close agreement between the analytical and empirical curves confirms the utility of the proposed reference model. From the results we can observe that if the vehicles are driven in the rightmost or the leftmost lane and close to the large objects such as highway dividers or sound blockers on the edge of the highway, the single-bounced rays bear more energy than the double-bounced rays. On the other hand, if the vehicles are driven in the middle lanes of the highway or in the urban environment [9], the double-bounced rays are prevalent.

The remainder of the paper is organized as follows. For ease of reference, Section II reviews our 3-D wideband MIMO M-to-M reference model. Section III describes the measurement campaign and the data processing techniques used to process the measured data. Section IV compares the analytical and empirical results for the sD-psd and the psds. Finally, Section V provides some concluding remarks.

II. A 3-D Theoretical Model for Wideband MIMO Mobile-to-Mobile Channels

This section describes our 3-D theoretical model for wideband MIMO M-to-M multipath fading channels proposed in [6]. We consider a wideband MIMO communication system with L_t transmit and L_r receive omnidirectional antenna elements. It is assumed that both the T_x and R_x are in motion and equipped with low elevation antennas. The radio propagation occurs in outdoor metropolitan environments that are characterized by 3-D non-isotropic scattering with either line-of-sight (LoS) or non-line-of-sight (NLoS) conditions between the T_x and R_x. The MIMO channel can be described by an $L_r \times L_t$ matrix $\mathbf{H}(t,\tau) = [h_{ij}(t,\tau)]_{L_r \times L_t}$ of the input delay-spread functions.

978-1-4244-2644-7/08/$25.00 ©2008 IEEE

The 3-D reference model is derived using the 3-D geometrical "concentric-cylinders" model shown in Fig. 1. Around the $\mathrm{T_x}$, M fixed omnidirectional scatterers occupy a volume between cylinders of radii R_{t1} and R_{t2}. It is assumed that the M scatterers lie on L cylindric surfaces of radii $R_{t1} \leq R_t^{(l)} \leq R_{t2}$, where $1 \leq l \leq L$. The l^{th} cylindric surface contains $M^{(l)}$ fixed omnidirectional scatterers, and the $(m,l)^{th}$ transmit scatterer is denoted by $S_T^{(m,l)}$. Similarly, around the $\mathrm{R_x}$, N fixed omnidirectional scatterers occupy a volume between cylinders of radii R_{r1} and R_{r2}. It is assumed that the N scatterers lie on K cylindric surfaces of radii $R_{r1} \leq R_r^{(k)} \leq R_{r2}$, where $1 \leq k \leq K$. The k^{th} cylindric surface contains $N^{(k)}$ fixed omnidirectional scatterers, and the $(n,k)^{th}$ receive scatterer is denoted by $S_R^{(n,k)}$. The parameters

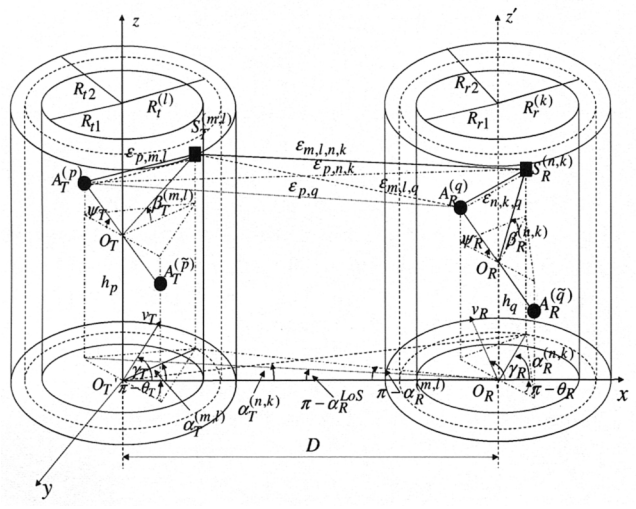

Fig. 1. The "concentric-cylinders" model with LoS, single- and double-bounced rays for a MIMO M-to-M channel with $L_t = L_r = 2$ antenna elements.

in Fig. 1 are defined in Table I. It is assumed that the radii R_{t2} and R_{r2} are sufficiently smaller than the distance D (local scattering condition). Furthermore, it is assumed that the distance D is smaller than $4R_{t1}R_{r1}L_r/(\lambda(L_t-1)(L_r-1))$ (channel does not experience keyhole behavior [10]), where λ denotes the carrier wavelength. Finally, it is assumed that d_T and d_R are much smaller than the radii R_{t1} and R_{r1}, i.e., $\max\{d_T, d_R\} \ll \min\{R_{t1}, R_{r1}\}$.

Observe from the 3-D geometrical model that some waves from the $\mathrm{T_x}$ antenna may traverse directly to the $\mathrm{R_x}$ antenna, while others are single- and/or double-bounced before arriving at the $\mathrm{R_x}$ antenna. Hence, the time-variant transfer function (i.e., the Fourier transform of the input delay-spread function) of the link $A_T^{(p)}$ - $A_R^{(q)}$ can be written as a superposition of the LoS, single-bounced transmit, single-bounced receive and double-bounced rays [6]

$$T_{pq}(t,f) = T_{pq}^{LoS}(t,f) + T_{pq}^{SBT}(t,f) + T_{pq}^{SBR}(t,f) + T_{pq}^{DB}(t,f). \quad (1)$$

The single-bounced, double-bounced, and LoS components of

TABLE I

DEFINITION OF PARAMETERS IN FIGURE 1.

D	The distance between the centers of the Tx and Rx cylinders.
$R_t^{(l)}, R_r^{(k)}$	The radius of the l^{th} Tx and k^{th} Rx cylinder, respectively.
d_T, d_R	The spacing between two adjacent antenna elements at the Tx and Rx, respectively.
θ_T, θ_R	The orientation of the Tx and Rx antenna array in the x-y plane (relative to the x-axis), respectively.
ψ_T, ψ_R	The elevation of the Tx's and Rx's antenna array relative to the x-y plane, respectively.
v_T, v_R	The velocities of the Tx and Rx, respectively.
γ_T, γ_R	The moving directions of the Tx and Rx, respectively.
$\alpha_T^{(m,l)}, \alpha_T^{(n,k)}$	The azimuth angles of departure (AAoD) of the waves that impinge on the scatterers $S_T^{(m,l)}$ and $S_R^{(n,k)}$, respectively.
$\alpha_R^{(m,l)}, \alpha_R^{(n,k)}$	The azimuth angles of arrival (AAoA) of the waves scattered from $S_T^{(m,l)}$ and $S_R^{(n,k)}$, respectively.
α_R^{LoS}	The AAoA of the LoS paths.
$\beta_T^{(m,l)}, \beta_R^{(n,k)}$	The elevation angles of departure (EAoD) and the elevation angles of arrival (EAoA), respectively.
$\varepsilon_{p,m,l}$, $\varepsilon_{m,l,q}$, $\varepsilon_{p,n,k}$, $\varepsilon_{n,k,q}$, $\varepsilon_{m,l,n,k}$ and ε_{pq}	The distances $d\left(A_T^{(p)}, S_T^{(m,l)}\right)$, $d\left(S_T^{(m,l)}, A_R^{(q)}\right)$, $d\left(A_T^{(p)}, S_R^{(n,k)}\right)$, $d\left(S_T^{(m)}, S_R^{(n)}\right)$, $d\left(S_R^{(n,k)}, A_R^{(q)}\right)$, $d\left(S_T^{(m,l)}, S_R^{(n,k)}\right)$, and $d\left(A_T^{(p)}, A_R^{(q)}\right)$, respectively
h_p, h_q	The distances $d\left(O_T, O_T'\right)$ and $d\left(O_R, O_R'\right)$, respectively.

the time-variant transfer function are, respectively,

$$T_{pq}^{SBT}(t,f) = \sqrt{\frac{\eta_T \Omega_{pq}}{K_{pq}+1}} \lim_{M\to\infty} \sum_{l=1}^{L} \sum_{m=1}^{M^{(l)}} \frac{\left(1-\frac{\gamma}{2}\frac{R_t^{(l)}}{D}\right)}{\sqrt{M}} a_{p,m,l}^{SBT} \times b_{q,m,l}^{SBT} e^{j2\pi t f_{T\max}\cos\left(\alpha_T^{(m,l)}-\gamma_T\right)\cos\beta_T^{(m,l)}} \times e^{j2\pi t f_{R\max}\left(\Delta_T^{(l)}\sin\gamma_R\sin\alpha_T^{(m,l)}-\cos\gamma_R\right)\cos\left(\Delta_T^{(l)}\beta_T^{(m,l)}+\Delta_H/D\right)} \times e^{-j\frac{2\pi}{c_0\cos\beta_T^{(m,l)}} f\left[D+R_t^{(l)}\left(1-\cos\alpha_T^{(m,l)}\right)\right]+j\phi_{m,l}}, \quad (2)$$

$$T_{pq}^{SBR}(t,f) = \sqrt{\frac{\eta_R \Omega_{pq}}{K_{pq}+1}} \lim_{N\to\infty} \sum_{k=1}^{K} \sum_{n=1}^{N^{(k)}} \frac{\left(1-\frac{\gamma}{2}\frac{R_r^{(k)}}{D}\right)}{\sqrt{N}} a_{p,n,k}^{SBR} \times b_{q,n,k}^{SBR} e^{j2\pi t f_{R\max}\cos\left(\alpha_R^{(n,k)}-\gamma_R\right)\cos\beta_R^{(n,k)}} \times e^{j2\pi t f_{T\max}\left(\Delta_R^{(k)}\sin\gamma_T\sin\alpha_R^{(n,k)}+\cos\gamma_T\right)\cos\left(\Delta_R^{(k)}\beta_R^{(n,k)}-\Delta_H/D\right)} \times e^{-j\frac{2\pi}{c_0\cos\beta_R^{(n,k)}} f\left[D+R_r^{(k)}\left(1+\cos\alpha_R^{(n,k)}\right)\right]+j\phi_{n,k}}, \quad (3)$$

$$T_{pq}^{DB}(t,f) = \sqrt{\frac{\eta_T R \Omega_{pq}}{K_{pq}+1}} \lim_{M,N\to\infty} \sum_{l,m=1}^{L,M^{(l)}} \sum_{k,n=1}^{K,N^{(k)}} \frac{\left(1-\frac{\gamma}{2}\frac{R_t^{(l)}+R_r^{(k)}}{2D}\right)}{\sqrt{MN}} a_{p,m,l}^{DB} b_{q,n,k}^{DB} e^{j2\pi t f_{T\max}\cos\left(\alpha_T^{(m,l)}-\gamma_T\right)\cos\beta_T^{(m,l)}} \times e^{j2\pi t f_{R\max}\cos\left(\alpha_R^{(n,k)}-\gamma_R\right)\cos\beta_R^{(n,k)}} \times e^{-j\frac{2\pi}{c_0} f\left[D+\frac{R_t^{(l)}\left(1-\cos\alpha_T^{(m,l)}\right)}{\cos\beta_T^{(m,l)}}+\frac{R_r^{(k)}\left(1+\cos\alpha_R^{(n,k)}\right)}{\cos\beta_R^{(n,k)}}\right]+j\phi_{m,l,n,k}}, \quad (4)$$

$$T_{pq}^{LoS}(t,f) = \sqrt{\frac{K_{pq}\Omega_{pq}}{1+K_{pq}}} e^{j2\pi t f_{T\max}\cos\left(\pi-\alpha_{Rq}^{LoS}-\gamma_T\right)} \times e^{j2\pi t f_{R\max}\cos\left(\alpha_{Rq}^{LoS}-\gamma_R\right)} e^{-j\frac{2\pi}{c_0} f\sqrt{D^2+\Delta_H{}^2}} e^{-j\frac{2\pi}{\lambda}D} \times e^{j\frac{2\pi}{\lambda}\left[(0.5L_t+0.5-p)d_{Tx}+(0.5L_r+0.5-q)d_R\cos\psi_R\cos(\alpha_{Rq}^{LoS}-\theta_R)\right]}. \quad (5)$$

In (2) – (5), K_{pq} denotes the Rice factor (ratio of LoS

to scatter received power) of the subchannel $A_T^{(p)} - A_R^{(q)}$, γ is the path loss exponent, λ is the carrier wavelength, c_0 is the speed of light, $f_{T\max} = v_T/\lambda$ and $f_{R\max} = v_R/\lambda$ are the maximum Doppler frequencies associated with the T_x and R_x, respectively, $\Delta_T^{(l)} = R_t^{(l)}/D$, $\Delta_R^{(k)} = R_r^{(k)}/D$, $\Delta_H = h_p - h_q$, $\Omega_{pq} = D^{-\gamma} P_{pq} \lambda^2/(4\pi)^2$, and P_{pq} is the power transmitted through the subchannel $A_T^{(p)} - A_R^{(q)}$. The parameters η_T, η_R, and η_{TR} specify how much the single- and double-bounced rays contribute in the total averaged power, i.e., these parameters satisfy $\eta_T + \eta_R + \eta_{TR} = 1$. Furthermore, the parameters p and q take values from the sets $p \in \{1, \ldots, L_t\}$ and $q \in \{1, \ldots, L_r\}$. Finally, the parameters $a_{p,m,l}^{SBT}$, $b_{q,m,l}^{SBT}$, $a_{p,n,k}^{SBR}$, $b_{q,n,k}^{SBR}$, $a_{p,m,l}^{DB}$, and $b_{q,n,k}^{DB}$ are, respectively,

$$a_{p,m,l}^{SBT} = e^{j\frac{2\pi}{\lambda}(0.5L_t+0.5-p)d_{Tx}\cos\alpha_T^{(m,l)}\cos\beta_T^{(m,l)}} \tag{6}$$
$$e^{j\frac{2\pi}{\lambda}(0.5L_t+0.5-p)\left[d_{Ty}\sin\alpha_T^{(m,l)}\cos\beta_T^{(m,l)}+d_{Tz}\sin\beta_T^{(m,l)}\right]}$$

$$b_{q,m,l}^{SBT} = e^{-j\frac{2\pi}{\lambda}\left(D+R_t^{(l)}\right)} \tag{7}$$
$$e^{j\frac{2\pi}{\lambda}(0.5L_r+0.5-q)d_R\cos\psi_R\rho_R\cos\left(\Delta_T^{(l)}\beta_T^{(m,l)}+\Delta_H/D\right)}$$

$$a_{p,n,k}^{SBR} = e^{-j\frac{2\pi}{\lambda}\left(D+R_r^{(k)}\right)} \tag{8}$$
$$e^{j\frac{2\pi}{\lambda}(0.5L_t+0.5-p)d_T\cos\psi_T\rho_T\cos\left(\Delta_R^{(k)}\beta_R^{(n,k)}-\Delta_H/D\right)}$$

$$b_{q,n,k}^{SBR} = e^{j\frac{2\pi}{\lambda}(0.5L_r+0.5-q)d_{Rx}\cos\alpha_R^{(n,k)}\cos\beta_R^{(n,k)}} \tag{9}$$
$$e^{j\frac{2\pi}{\lambda}(0.5L_r+0.5-q)\left[d_{Ry}\sin\alpha_R^{(n,k)}\cos\beta_R^{(n,k)}+d_{Rz}\sin\beta_R^{(n,k)}\right]}$$

$$a_{p,m,l}^{DB} = e^{-j\frac{2\pi}{\lambda}\left(D/2+R_t^{(l)}\right)} e^{j\frac{2\pi}{\lambda}(0.5L_t+0.5-p)d_{Tz}\sin\beta_T^{(m,l)}} \tag{10}$$
$$e^{j\frac{2\pi}{\lambda}(0.5L_t+0.5-p)\left[d_{Tx}\cos\alpha_T^{(m,l)}\cos\beta_T^{(m,l)}+d_{Ty}\sin\alpha_T^{(m,l)}\cos\beta_T^{(m,l)}\right]}$$

$$b_{q,n,k}^{DB} = e^{-j\frac{2\pi}{\lambda}\left(D/2+R_r^{(k)}\right)} e^{j\frac{2\pi}{\lambda}(0.5L_r+0.5-q)d_{Rz}\sin\beta_R^{(n,k)}} \tag{11}$$
$$e^{j\frac{2\pi}{\lambda}(0.5L_r+0.5-q)\left[d_{Rx}\cos\alpha_R^{(n,k)}\cos\beta_R^{(n,k)}+d_{Ry}\sin\alpha_R^{(n,k)}\cos\beta_R^{(n,k)}\right]}$$

where $d_{Tx} = d_T\cos\psi_T\cos\theta_T$, $d_{Ty} = d_T\cos\psi_T\sin\theta_T$, $d_{Tz} = d_T\sin\psi_T$, $d_{Rx} = d_R\cos\psi_R\cos\theta_R$, $d_{Ry} = d_R\cos\psi_R\sin\theta_R$, $d_{Rz} = d_R\sin\psi_R$, $\rho_R = \Delta_T^{(l)}\sin\theta_R\sin\alpha_T^{(m,l)} - \cos\theta_R$, $\rho_T = \Delta_R^{(k)}\sin\theta_T\sin\alpha_R^{(n,k)} + \cos\theta_T$.

The model in [6] assumes that the angles of departure and the angles of arrival are random variables. Furthermore, it assumes that the phases ϕ_m, ϕ_n, and ϕ_{mn} are also random variables uniformly distributed on the interval $[-\pi, \pi)$ and independent from the angles of departure and the angles of arrival. The azimuth angles of departure and arrival, $\alpha_T^{(m,l)}$ and $\alpha_R^{(n,k)}$, are characterized by the von Mises probability density function (pdf) [11]. The elevation angles of departure and arrival, $\beta_T^{(m,l)}$ and $\beta_R^{(n,k)}$, are characterized by the pdf [12] $f(\varphi) = \pi\cos(\pi\varphi/(4\varphi_m))/(4|\varphi_m|)$ for $|\varphi| \leq |\varphi_m| \leq \pi/2$ and $f(\varphi) = 0$ otherwise. The parameter φ_m is the maximum elevation angle and lies in the range $0° \leq |\varphi_m| \leq 20°$ [13], [6]. Finally, the radii $R_t^{(l)}$ and $R_r^{(k)}$ are characterized by the pdf $f(R) = 2R/(R_2^2 - R_1^2)$ [6].

III. Measurement Campaign Description and Data Processing

This section describes our MIMO M-to-M channel-sounding experimental campaign and the signal processing techniques used to process the collected data.

The MIMO M-to-M channel-sounding experimental campaign was conducted on the Interstate highways in the midtown Atlanta metropolitan area. Each van was equipped with a linear antenna array, consisting of four vertically-polarized, magnetic-mount, 2.435 GHz antenna elements. The antenna elements were placed across the roof of the van from the passenger side of the van to the driver side of the van and spaced 2.943 wavelengths apart from each other. The vans were usually driven in a convoy fashion (in the same lane and at the same speed), roughly 100 m to 300 m apart, and with speeds up to 60 mph.

Channel sounding waveforms were transmitted from the trailing vehicle and the signals were received and recorded by the leading vehicle. Video cameras were used in the vehicles to provide indications of time, velocity, and location, to support post-test processing of the collected data. The measurements typically included both LoS and NLoS conditions, as other vehicles and obstructions often masked the direct LoS. Details associated with the measurement campaign are summarized in Table II. Finally, Figs. 2 and 3 show photographs of two different locations where the data used in the paper were collected.

TABLE II

Description of the Measurement Campaign.

Carrier Frequency	2.435 GHz
Signal Modulation	OFDM symbols with 256 subcarriers
Transmit Sample Rate (used to generate the OFDM signal)	18 MHz
Transmit Waveform pulse repetition interval	The pulse repetition interval of the sounding waveform was approximately 300 microseconds
Frequency Synchronization	Rubidium clocks at the transmitter and the receiver
Data collection System	Pentek-based VME custom collection system with Mercury Computer Systems RF front ends; 4-channel receiver with pairwise sample synchronization
Data collection products at the receiver per snapshot (corresponding roughly to 3-second durations of contiguous data)	Approximately 55M contiguous complex baseband samples per antenna output
Collection Scenario with mobile vans	Vans traveling 30 to 60 mph in the same direction and within 100 m to 300m apart on the I75 Expressway.

Our wideband channel model is focused on characterizing the fast-fading characteristics of the channel. To allow fair comparison between our wideband channel model and the measured data, the slow-fading component of the measured signal envelope is removed. This is achieved using the local sliding window technique [14], where the sliding window length is set to 20λ. Furthermore, to allow comparison between the theoretical normalized space-time-frequency correlation function (STF-CF) in [6] and the STF-CF obtained from measured data, the power of each measured subchannel $A_T^{(p)}$ - $A_R^{(q)}$ is normalized to unity. This normalization is performed as follows:

$$\hat{h}_{pq}(n\Delta t_s, k\Delta\tau_s) = \frac{h_{pq}(n\Delta t_s, k\Delta\tau_s)}{\hat{\sigma}_{pq}(k\Delta\tau_s)}, \tag{12}$$

where $h_{pq}(n\Delta t_s, k\Delta\tau_s)$ is the measured input delay-spread function, Δt_s and N_t denote the sampling period and the

number of samples with respect to the time variable t, $\Delta\tau_s$ and N_τ denote the sampling period and the number of samples with respect to the delay variable τ, $n \in \{0, \ldots, N_t - 1\}$, $k \in \{0, \ldots, N_\tau - 1\}$, and $\hat{\sigma}^2_{pq}(k\Delta\tau_s)$ is the estimated variance of the measured $A_T^{(p)}$ - $A_R^{(q)}$ subchannel, respectively. The estimated variance is calculated as $\hat{\sigma}^2_{pq}(k\Delta\tau_s) = N_t^{-1} \sum_{n=0}^{N_t-1} |h_{pq}(n\Delta t_s, k\Delta\tau_s) - \hat{m}_{pq}(k\Delta\tau_s)|^2$, where $\hat{m}_{pq}(k\Delta\tau_s)$ is the estimated mean.

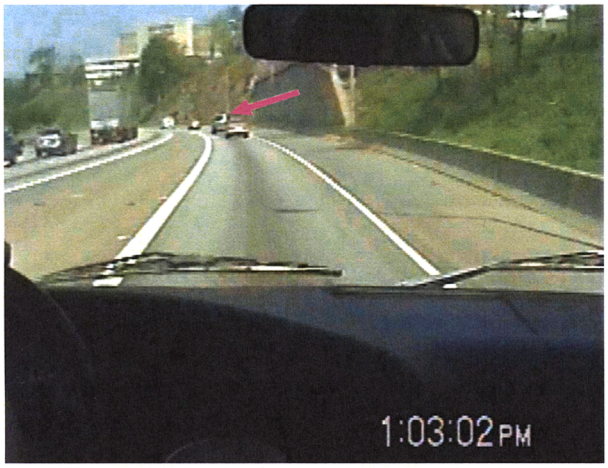

Fig. 2. Photograph of the leading van, taken from the trailing van on the highway in the midtown Atlanta metropolitan area. The vehicles are driven in the rightmost lane of the highway.

From the normalized input delay-spread function, the sD-psd is calculated using the Welch algorithm [15]. The psds is obtained by averaging the squared magnitudes of the normalized input delay-spread function $\hat{h}_{pq}(n\Delta t_s, k\Delta\tau_s)$ over all times $n\Delta t_s$.

IV. Reference Model Validation

In this section, we compare the sD-psd and the psds obtained from the reference model with those obtained from the measurement campaign described in Section III. The expressions for the theoretical sD-psd and psds are derived in [6], [7]. The wideband channel measurements collected on the Interstate highway were performed at 2.435 GHz and the moving directions were $\gamma_T = \gamma_R = 90°$. The antenna array elements at both vehicles have the azimuth and elevation angles $\theta_T = \theta_R = 0°$ and $\psi_T = \psi_R = 0°$, respectively. All antenna elements have the same height, $\Delta_H = 0$, and the distance between the antenna elements is $d_T = d_R = 2.943\ \lambda$. It is assumed that the path loss exponent γ is 4.

Figs. 4 and 5 compare the theoretical sD-psd and psds with the measured sD-psd and psds collected at the location shown in Fig. 2. The analytical curves are obtained with the parameters $\beta_{Tm} = 7.4°$, $\beta_{Rm} = 8.3°$, $\mu_T = 101.4°$, $\mu_R = 281.5°$, $k_T = 5.5$, $k_R = 5.2$, $\eta_T = 0.358$, $\eta_R = 0.288$, $\eta_{TR} = 0.354$, $R_{t1} = R_{r1} = 4.5$ m, $R_{t2} = R_{r2} = 45$ m, and $K = 1.29$. These parameters are estimated using the method in [16]. The maximum Doppler frequencies were $f_{T\max} = f_{R\max} = 181.72$ Hz and the distance between the

Fig. 3. Photograph of the leading van, taken from the trailing van on the highway in the midtown Atlanta metropolitan area. The vehicles are driven in the middle lanes of the highway.

T_x and R_x was approximately $D = 180$ m. In this set of data, the single-bounced rays are more dominant than the double-bounced rays. This effect can be explained by the fact that both vans were in the rightmost lane and very close to the sound blockers on the edge of the highway (see Fig. 2).

Figs. 6 and 7 compare the theoretical sD-psd and psds with the measured sD-psd and psds collected at the location shown in Fig. 3. The analytical curves are obtained with the parameters $\beta_{Tm} = 10.2°$, $\beta_{Rm} = 10.3°$, $\mu_T = 90.3°$, $\mu_R = 271.3°$, $k_T = 9.5$, $k_R = 10.3$, $\eta_T = 0.141$, $\eta_R = 0.037$, $\eta_{TR} = 0.822$, $R_{t1} = R_{r1} = 4$ m, $R_{t2} = R_{r2} = 40$ m, and $K = 2.341$. The maximum Doppler frequencies were $f_{T\max} = f_{R\max} = 199.89$ Hz and the distance between the T_x and R_x was approximately $D = 147.52$ m. In this set of data, the double-bounced rays are prevalent because the vehicles are driven in the middle lane of the highway.

Figs. 4 - 7 show close agreement between the theoretical and empirical curves. These results confirm the utility of the proposed model and show that if the vehicles are driven in the rightmost or the leftmost lane and close to the large objects such as highway dividers or sound blockers on the edge of the highway, the single-bounced rays bear more energy than the double-bounced rays. However, if the vehicles are driven in the middle lanes of the highway, the double-bounced rays are prevalent.

V. Conclusions

This paper reviewed our 3-D reference model for wideband MIMO M-to-M channels. To validate this model, a MIMO M-to-M channel-sounding experimental campaign was conducted along expressways in the Atlanta metropolitan area. The measured data was processed and compared with the analytical predictions. The close agreement between the analytical and empirical curves confirms the utility of the proposed reference model.

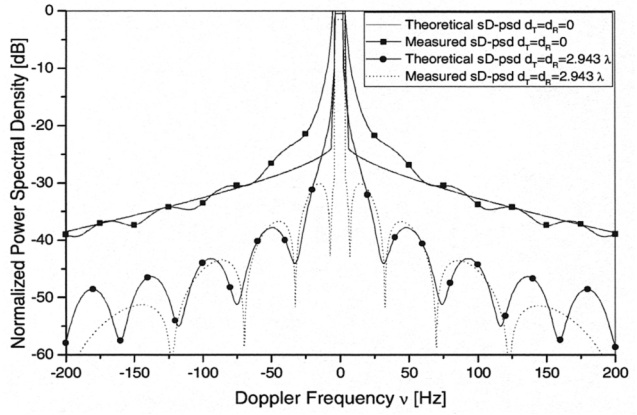

Fig. 4. The theoretical and the measured sD-psd on the highway, when the vehicles are driven in the rightmost lane of the highway.

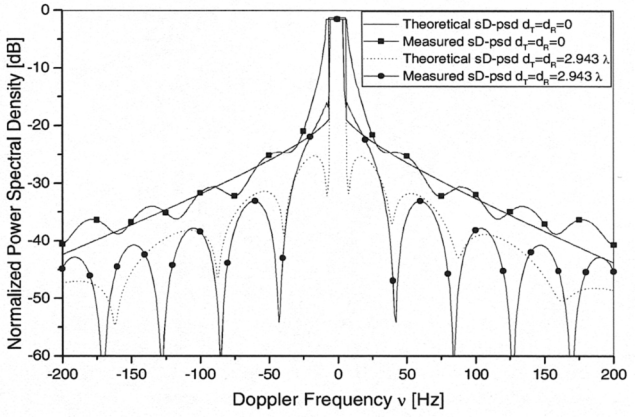

Fig. 6. The theoretical and the measured sD-psd on the highway, when the vehicles are driven in the middle lanes of the highway.

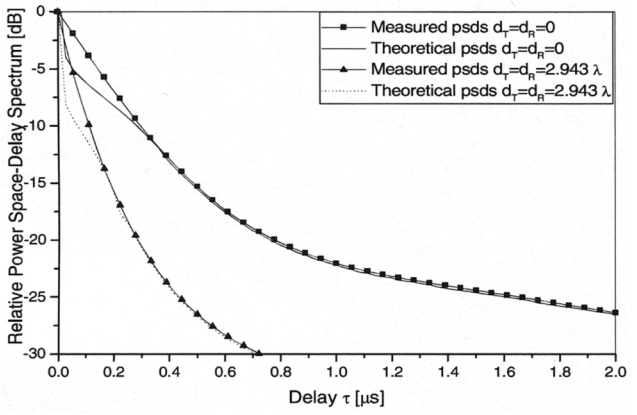

Fig. 5. The theoretical and the measured psds on the highway, when the vehicles are driven in the rightmost lane of the highway.

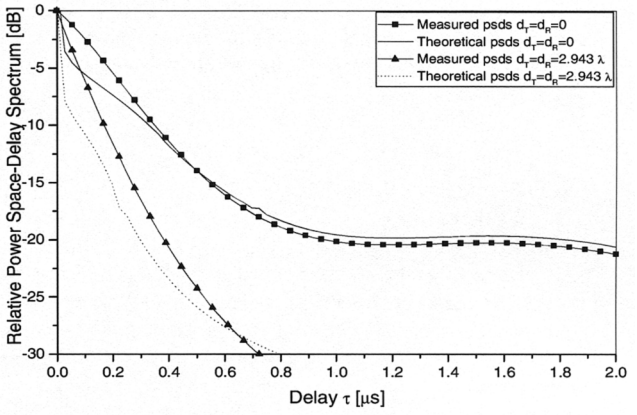

Fig. 7. The theoretical and the measured psds on the highway, when the vehicles are driven in the middle lanes of the highway.

DISCLAIMER

The views and conclusions contained in this document are those of the authors and should not be interpreted as representing the official policies, either expressed or implied, of the Army Research Laboratory or the U. S. Government.

REFERENCES

[1] A. S. Akki and F. Haber, "A statistical model for mobile-to-mobile land communication channel," *IEEE Trans. on Veh. Tech.*, vol. 35, pp. 2–10, Feb. 1986.

[2] J. Maurer, T. Fügen, and W. Wiesbeck, "Narrow-band measurement and analysis of the inter-vehicle transmission channel at 5.2 GHz,"*Proc. IEEE VTC*, pp. 1274–1278, Birmingham, AL, USA, May 2002.

[3] G. Acosta, K. Tokuda, and M. A. Ingram, "Measured joint Doppler-delay power profiles for vehicle-to-vehicle communications at 2.4 GHz," *Proc. IEEE GLOBECOM*, pp. 3813–3817, Dallas, TX, USA, Nov. 2004.

[4] M. Pätzold, B.O. Hogstad, N. Youssef, and D. Kim, "A MIMO mobile-to-mobile channel model: Part I-the reference model," *Proc. IEEE PIMRC*, pp. 573–578, Berlin, Germany, Sept. 2005.

[5] A.G. Zajić and G.L. Stüber, "A three-dimensional MIMO mobile-to-mobile channel model," *IEEE WCNC*, Hong Kong, Mar. 2007.

[6] A.G. Zajić and G.L. Stüber, "A three dimensional parametric model for wideband MIMO mobile-to-mobile channels," *Proc. IEEE GLOBECOM*, Washington, D.C., USA, Nov. 2007.

[7] A.G. Zajić and G.L. Stüber, "Statistical properties of wideband MIMO mobile-to-mobile channels," *IEEE WCNC*, Las Vegas, NE, Mar. 2008.

[8] A.G. Zajić and G.L. Stüber, "A 3-D simulation models for wideband MIMO mobile-to-mobile channels," *Proc. IEEE MILCOM*, Orlando, FL, USA, Oct. 2007.

[9] A.G. Zajić, G.L. Stüber, Thomas G. Pratt, and Son Nguyen, "Statistical modeling and experimental verification of wideband MIMO mobile-to-mobile channels in urban environments,"*Proc. 15th ICT*, June 2008.

[10] D. Gesbert, H. Bölcskei, D.A. Gore, and A.J. Paulraj, "Outdoor MIMO wireless channels: models and performance prediction," *IEEE Trans. on Commun.*, vol. 50, pp. 1926–1934, Dec. 2002.

[11] A. Abdi, J. A. Barger, and M. Kaveh, "A parametric model for the distribution of the angle of arrival and the associated correlation function and power spectrum at the mobile station," *IEEE Trans. on Veh. Tech.*, vol. 51, pp. 425–434, May 2002.

[12] J.D. Parsons and A.M.D. Turkmani, "Characterisation of mobile radio signals: model description," *IEE Proc. I, Commun., Speach, and Vision*, vol. 138, pp. 549–556, Dec. 1991.

[13] A. Kuchar, J.-P. Rossi, and E. Bonek, "Directional macro-cell channel characterization from urban measurements," *IEEE Trans. on Antennas and Propagation*, vol. 48, pp. 137–146, Feb. 2000.

[14] W. C. Y. Lee,"Estimate of local average power of mobile radio signal," *IEEE Trans. on Veh. Tech.*, vol. 34, pp. 22–27, Feb. 1985.

[15] P. D. Welch, "The use of fast fourier transform for the estimation of power spectra: a method based on time averaging over short, modified periodograms," *IEEE Trans. Audio Electroacoustics*, vol. AU-15, pp. 70–73, June 1967.

[16] A.G. Zajić, G.L. Stüber, Thomas G. Pratt, and Son Nguyen, "Wideband MIMO mobile-to-mobile channels: statistical modeling with experimental verification," accepted with minor revisions in *Proc. IEEE Trans. on Veh. Tech*, Apr. 2008.